Pramana – J. Phys. (2019) 93:95
https://doi.org/10.1007/s12043-019-1848-6

Consequences of chemical reaction in temperature-dependent thermal conductivity fluid flow by a rotating disk with variable thickness

MARIA IMTIAZ[1,*], FIZA SHAHID[2], TASAWAR HAYAT[2,3] and AHMED ALSAEDI[3]

[1]Department of Social and Behavioral Sciences, National University of Medical Sciences, Rawalpindi, Pakistan
[2]Department of Mathematics, Quaid-I-Azam University 45320, Islamabad 44000, Pakistan
[3]Nonlinear Analysis and Applied Mathematics (NAAM) Research Group, Department of Mathematics, Faculty of Science, King Abdulaziz University 80203, Jeddah 21589, Saudi Arabia
*Corresponding author. E-mail: mi_qau@yahoo.com

MS received 11 April 2019; revised 11 June 2019; accepted 27 June 2019

Abstract. This paper examines the steady flow due to a rotating disk with variable thickness. Equations are modelled by considering the homogeneous–heterogeneous reactions and variable thermal conductivity. The modified Von Karman transformations are utilised to convert the governing partial differential equations into dimensionless nonlinear ordinary differential equations. Convergent series solutions are computed. The impact of relevant parameters on flow fields is computed and interpreted. It is predicted that an increase in disk thickness index decreases the axial velocity while increases the radial and tangential velocities. The Nusselt number enhances by increasing the thickness parameter of a disk.

Keywords. Homogeneous–heterogeneous reactions; variable thickness; variable thermal conductivity; rotating disk.

PACS Nos 44.25.+f; 47.10.A; 47.10.ad; 47.15.G; 47.27.Ak

1. Introduction

Heat transfer through a rotating disk has become a compelling research topic owing to its theoretical and practical values. Fluid flow in rotating media has a pivotal role in systems which generate power, medical equipments, air cleaning machines, gas turbines, food processing machines and electrical and aerodynamical engineering. A seminal contribution in the study of fluid flow by an infinite rotating disk was made by Karman [1]. He developed appropriate transformations that have been utilised later in transforming partial differential equations to a set of non-dimensionalised equations. Viscous fluid flow concerning two coaxial rotating disks was presented by Stewartson [2]. Kumar *et al* [3] analysed the magnetohydrodynamics (MHD) flow of a fluid that is confined between the solid and porous rotating disks. Ming *et al* [4] explored the steady flow and heat transfer of the power-law fluid over a rotating disk. Turkyilmazoglu [5] examined the rate of heat transfer of fluid flow induced by a rotating disk with shrinking effect. Nanofluid flow past a vertical plate in a rotating system with thermal radiation effects has been discussed by Narayana *et al* [6]. Flow of Ostwald–de Waele fluid over a variable thickness rotating disk with variable thickness index decreasing was discussed by Xun *et al* [7].

The heat transfer phenomenon over the rotating disk has a range of real-life applications in several technological and industrial procedures including nuclear reactors, microelectronics, transportations, fuel cells, pasteurisation of food, hybrid powered engines and pharmaceutical processes. These processes involve many thermophysical properties that are generally supposed to be constant. Practically, the most desired physical property for such situations is the temperature-dependent thermal conductivity. Thermal conductivity changes linearly from 0 to 400 F for liquid metals [8–15].

Surfaces with variable thickness have fascinating applications in technology, particularly in civil,

Published online: 04 October 2019

mechanical, architectural and aeronautical processes. This property causes a significant reduction in surface weight and helps in improving its utilisation [16]. Flow by a continuously stretching sheet of variable thickness was examined by Fang *et al* [17]. The analysis of thermal diffusive flow caused by a stretching sheet with variable thickness was made by Subhashini *et al* [18]. Hayat *et al* [19] analysed the influence of Cattaneo–Christov heat flux model on the flow induced by a stretching sheet of variable thickness. Hayat *et al* [20] studied the flow of Williomson nanofluid over a stretching sheet of variable thickness.

Some chemical reactions require catalyst to proceed and have no capability to initiate the process on their own. The homogeneous–heterogeneous chemical reactions usually occur in combustion, catalysis and biochemical procedure. There exists a strong association between the homogeneous reaction occurring in fluid bulk and the heterogeneous reaction that arises on some catalytic surface. A model of boundary layer flow by a flat plate with effects of homogeneous–heterogeneous reactions was presented by Merkin [21]. He observed the surface reaction to be more dominating, close to the leading edge of a plate. The homogeneous–heterogeneous reactions with same diffusivities of reactants and autocatalysts were discussed by Chaudhary and Merkin [22]. Khan and Pop [23] studied the impact of homogeneous–heterogeneous reactions on forced convection flow near the forward stagnation point. Hayat *et al* [24] explored the couple stress fluid flow with chemical reactions. The impact of homogeneous and heterogeneous reactions on viscoelastic fluid flow has been examined by Khan and Pop [25]. Hayat *et al* [26] studied the influence of homogeneous–heterogeneous reactions in peristalsis through curved geometry. The homogeneous–heterogeneous reactions and Cattaneo–Christov heat flux in MHD flow of Oldroyd-B fluid are inspected by Hayat *et al* [27]. Hayat *et al* [28] reported the effects of chemical reactions on Jeffrey fluid flow in the presence of Cattaneo–Christov heat flux. Theoretical investigation of chemically reactive flow of water-based carbon nanotubes (single walled and multiple walled) with melting heat transfer was analysed by Hayat *et al* [29].

The purpose of the present work is to analyse the fluid flow induced by a rotating disk of variable thickness. The mass and heat transfer are analysed in the presence of temperature-dependent thermal conductivity and the homogeneous–heterogeneous reactions. Convergent series solutions are obtained by homotopy analysis method [30–35]. The effects of relevant parameters on velocity, temperature and concentration profiles are examined graphically.

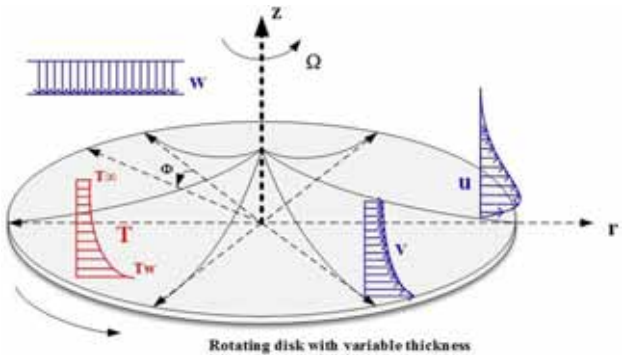

Figure 1. Flow geometry.

2. Formulation

Let us consider the three-dimensional steady flow of viscous fluid with variable thermal conductivity induced by a rotating disk. The disk is of variable thickness and is rotating with angular velocity Ω. The temperature of the disk is T_w and the ambient temperature is T_∞. Here cylindrical coordinates (r, θ, z) are used (see figure 1).

We considered the model for homogeneous–heterogeneous reactions as suggested by Chaudhary and Merkin [22]. For cubic autocatalysis, the homogeneous reaction is as follows:

$$A_1 + 2A_2 \to 3A_2, \quad \text{rate} = k_c a b^2, \tag{1}$$

while on the catalyst surface the heterogeneous reaction is

$$A_1 \to A_2, \quad \text{rate} = k_s a, \tag{2}$$

where a and b are the concentrations of the chemical species A_1 and A_2, respectively, while k_c and k_s are the rate constants. Also, these reactions are assumed to be isothermal. By assuming $\partial p/\partial r = \partial p/\partial z = 0$, the modelled equations are as follows:

$$\frac{\partial u}{\partial r} + \frac{\partial w}{\partial z} + \frac{u}{r} = 0, \tag{3}$$

$$\rho\left(u\frac{\partial u}{\partial r} + w\frac{\partial u}{\partial z} - \frac{v^2}{r}\right) = \mu\left(\frac{\partial^2 u}{\partial r^2} + \frac{\partial^2 u}{\partial z^2} - \frac{u}{r^2} + \frac{1}{r}\frac{\partial u}{\partial r}\right), \tag{4}$$

$$\rho\left(w\frac{\partial v}{\partial z} + u\frac{\partial v}{\partial r} + \frac{uv}{r}\right) = \mu\left(\frac{\partial^2 v}{\partial z^2} + \frac{\partial^2 v}{\partial r^2} - \frac{v}{r^2} + \frac{1}{r}\frac{\partial v}{\partial r}\right), \tag{5}$$

$$\rho\left(w\frac{\partial w}{\partial z}+u\frac{\partial w}{\partial r}\right)=\mu\left(\frac{\partial^2 w}{\partial r^2}+\frac{1}{r}\frac{\partial w}{\partial r}+\frac{\partial^2 w}{\partial z^2}\right), \quad (6)$$

$$\rho c_p\left(w\frac{\partial T}{\partial z}+u\frac{\partial T}{\partial r}\right)=\frac{\partial}{\partial z}\left(k(T)\frac{\partial T}{\partial z}\right)+\frac{\partial}{\partial r}\left(k(T)\frac{\partial T}{\partial r}\right)+\frac{1}{r}k(T)\frac{\partial T}{\partial r}, \quad (7)$$

$$u\frac{\partial a}{\partial r}+w\frac{\partial a}{\partial z}=D_{A_1}\left(\frac{\partial^2 a}{\partial r^2}+\frac{\partial^2 a}{\partial z^2}+\frac{1}{r}\frac{\partial a}{\partial r}\right)-k_c a b^2, \quad (8)$$

$$w\frac{\partial b}{\partial z}+u\frac{\partial b}{\partial r}=D_{A_2}\left(\frac{\partial^2 b}{\partial r^2}+\frac{\partial^2 b}{\partial z^2}+\frac{1}{r}\frac{\partial b}{\partial r}\right)+k_c a b^2. \quad (9)$$

The related boundary conditions are

$$u=0,\quad v=\Omega r,\quad w=0,\quad T=T_w,$$

$$D_{A_1}\frac{\partial a}{\partial z}=k_s a,\quad D_{A_2}\frac{\partial b}{\partial z}=-k_s a$$

$$\text{at } z=A\left(\frac{r}{R_0}+1\right)^{-m},$$

$$u\to 0,\quad v\to 0,\quad T\to T_\infty,\quad a\to a_0,$$

$$b\to 0 \quad \text{as} \quad z\to\infty, \quad (10)$$

where u, v, w are the components of velocity in the (r, θ, z) direction, respectively, ρ is the density, c_p is the specific heat, μ is the dynamic viscosity, p is the pressure, D_{A_1} and D_{A_2} are the diffusion coefficients, m is the disk thickness index and R_0 is the feature radius. Also, $k(T)$ is the thermal conductivity, which depends on temperature. This temperature-dependent thermal conductivity is approximated as follows:

$$k(T)=k_{\tilde{a}}(1+\tilde{b}(T-T_\infty)), \quad (11)$$

where $\tilde{b}$ is the temperature coefficient of thermal conductivity and $k_{\tilde{a}}$ is the thermal conductivity at reference temperature. We consider the following transformations:

$$u=r\Omega F(\eta),\quad v=r\Omega G(\eta),$$

$$w=R_0\Omega\left(\frac{\Omega R_0^2\rho}{\mu}\right)^{-1/(n+1)}\left(1+\frac{r}{R_0}\right)^{-m}H(\eta),$$

$$\Phi(\eta)=\frac{a}{a_0},\quad \xi(\eta)=\frac{b}{a_0},\quad T=(T_w-T_\infty)\Theta+T_\infty,$$

$$\eta=\frac{z}{R_0}\left(\frac{\Omega R_0^2\rho}{\mu}\right)^{1/(n+1)}\left(1+\frac{r}{R_0}\right)^{m}. \quad (12)$$

Using these transformations, eqs (3)–(9) become

$$H'+2F+\eta m\epsilon F'=0, \quad (13)$$

$$\mathrm{Re}^{(1+n)/(1-n)}(1+r')^{2m}F''-HF'-F^2+G^2-\eta m\epsilon FF'=0, \quad (14)$$

$$\mathrm{Re}^{(1+n)/(1-n)}(1+r')^{2m}G''-HG'-2FG-\eta m\epsilon FF'=0, \quad (15)$$

$$\mathrm{Re}^{(1+n)/(1-n)}(1+r')^{2m}\frac{\gamma}{\mathrm{Pr}}\left(\Theta'^2+\frac{\Theta''}{\gamma}+\Theta\Theta''\right)-H\Theta'-\eta m\epsilon F\Theta'=0, \quad (16)$$

$$\frac{1}{\mathrm{Sc}}\mathrm{Re}^{(1+n)/(1-n)}(1+r')^{2m}\Phi''-H\Phi'-\eta m\epsilon\Phi'-k_1\Phi\xi^2=0, \quad (17)$$

$$\frac{\delta_1}{\mathrm{Sc}}\mathrm{Re}^{(1+n)/(1-n)}(1+r')^{2m}\xi''-H\xi'-\eta m\epsilon\xi'-k_1\Phi\xi^2=0 \quad (18)$$

and boundary conditions (10) take the form

$$H(\alpha)=0,\quad F(\alpha)=0,\quad G(\alpha)=1,\quad \Theta(\alpha)=1,$$

$$\mathrm{Re}^{(1-n)/2(1+n)}(1+r')^m\Phi'(\alpha)=k_2\Phi(\alpha),$$

$$\delta_1\mathrm{Re}^{(1-n)/2(1+n)}(1+r')^m\xi'(\alpha)=-k_2\Phi(\alpha),$$

$$F(\infty)\to 0,\quad G(\infty)\to 0,\quad \Theta(\infty)\to 0,$$

$$\Phi(\infty)\to 1,\quad \xi(\infty)\to 0, \quad (19)$$

where n is the power-law exponent of the fluid, $\epsilon = r/(r+R_0)$ is the dimensionless constant, $\mathrm{Re}=\Omega R_0^2/\nu$ is the Reynolds number, $r'=r/R_0$ is the dimensionless radius, $\gamma=\tilde{b}(T_w-T_\infty)$ is the dimensionless slope of thermal conductivity–temperature curve, $\mathrm{Pr}=\nu/\alpha$ is the Prandtl number, $\alpha=(A/R_0)(\Omega R_0^2\rho/\mu)^{1/(n+1)}$ is the disk thickness coefficient, $\mathrm{Sc}=\nu/D_{A_1}$ is the Schmidt number, $k_1=k_c a_0^2/\Omega$ is the homogeneous reaction parameter, $\delta_1=D_{A_1}/D_{A_2}$ is the ratio of diffusion coefficient and $k_2=(k_s\sqrt{\nu}/D_{A_1}\sqrt{\Omega})$ is the heterogeneous reaction parameter. The diffusion coefficients D_{A_1} and D_{A_2} are assumed to be of comparable value and hence the ratio of diffusion coefficients reduces to 1, i.e. $\delta=1$ and thus

$$\Phi(\eta)+\xi(\eta)=1. \quad (20)$$

Then eqs (17) and (18) become

$$\frac{1}{\mathrm{Sc}}\mathrm{Re}^{(1+n)/(1-n)}(1+r')^{2m}\Phi'' - H\Phi' - \eta m\epsilon\Phi' - k_1\Phi(1-\Phi)^2 = 0 \tag{21}$$

with boundary conditions

$$\mathrm{Re}^{(1-n)/2(1+n)}(1+r')^m\Phi'(\alpha) = k_2\Phi(\alpha), \quad \Phi(\infty)\to 1. \tag{22}$$

Considering

$$H(\eta) = h(\eta-\alpha) = h(\zeta), \tag{23}$$

$$F(\eta) = f(\eta-\alpha) = f(\zeta), \tag{24}$$

$$G(\eta) = g(\eta-\alpha) = g(\zeta), \tag{25}$$

$$\Theta(\eta) = \theta(\eta-\alpha) = \theta(\zeta), \tag{26}$$

$$\Phi(\eta) = \phi(\eta-\alpha) = \phi(\zeta), \tag{27}$$

eqs (13)–(19) are reduced to

$$h' + 2f + (\zeta+\alpha)m\epsilon f' = 0, \tag{28}$$

$$\mathrm{Re}^{(1+n)/(1-n)}(1+r')^{2m}f'' - hf' - f^2 + g^2 - (\zeta+\alpha)m\epsilon ff' = 0, \tag{29}$$

$$\mathrm{Re}^{(1+n)/(1-n)}(1+r')^{2m}g'' - hg' - 2fg - (\zeta+\alpha)m\epsilon fg' = 0, \tag{30}$$

$$\frac{\gamma}{\mathrm{Pr}}\mathrm{Re}^{(1+n)/(1-n)}(1+r')^{2m}\left(\theta'^2 + \frac{\theta''}{\gamma} + \theta\theta''\right) - h\theta' - (\zeta+\alpha)m\epsilon f\theta' = 0, \tag{31}$$

$$\frac{1}{\mathrm{Sc}}\mathrm{Re}^{(1+n)/(1-n)}(1+r')^{2m}\phi'' - h\phi' - (\zeta+\alpha)m\epsilon\phi' - k_1\phi(1-\phi)^2 = 0, \tag{32}$$

with boundary conditions

$$h(0)=0, \quad f(0)=0, \quad g(0)=1, \quad \theta(0)=1,$$
$$\mathrm{Re}^{(1-n)/(1+n)}(1+r')^{2m}\phi'(0) = k_2\phi(0),$$
$$f(\infty)\to 0, \quad g(\infty)\to 0,$$
$$\theta(\infty)\to 0, \quad \phi(\infty)\to 1. \tag{33}$$

Here the local skin friction coefficient (C_f) and the Nusselt number (Nu_r) are given by

$$C_f = \frac{\sqrt{\tau_{rz}^2+\tau_{\theta z}^2}}{\rho(r\Omega)^2}, \quad \mathrm{Nu}_r = \frac{rq_w}{k_{\tilde{a}}(T_w - T_\infty)}, \tag{34}$$

where τ_{rz} is the surface radial stress, $\tau_{\theta z}$ is the surface tangential stress and q_w is the surface heat flux which are given as

$$\tau_{rz} = \mu\left.\frac{\partial u}{\partial z}\right|_{z=A((r/R_0)+1)^{-m}},$$
$$\tau_{\theta z} = \mu\left.\frac{\partial v}{\partial z}\right|_{z=A((r/R_0)+1)^{-m}},$$
$$q_w = -k(T)\left.\frac{\partial T}{\partial z}\right|_{z=A((r/R_0)+1)^{-m}}. \tag{35}$$

The dimensionless local skin friction coefficient C_f and the Nusselt number Nu_r can be written as

$$C_f\mathrm{Re}^{n/(n+1)} = \frac{(1+r')^m}{r'}\sqrt{[f'(0)]^2+[g'(0)]^2},$$
$$\mathrm{Nu}_r\mathrm{Re}^{-1/(n+1)} = -r'(1+r')^m(1+\epsilon\theta)\left.\frac{\mathrm{d}\theta}{\mathrm{d}\zeta}\right|_{\zeta=0}. \tag{36}$$

3. Solutions procedure

3.1 *Zeroth-order deformation problems*

Let H_0, f_0, g_0, θ_0 and Φ_0 be the initial approximations taken in the following forms:

$$h_0(\zeta) = 0, \quad f_0(\zeta) = \zeta\mathrm{e}^{-\zeta}, \quad g_0(\zeta) = \mathrm{e}^{-\zeta},$$
$$\theta_0(\zeta) = \mathrm{e}^{-\zeta},$$
$$\phi_0(\zeta) = 1 - \frac{k_2}{\mathrm{Re}^{(1-n)/2(1+n)}(1+r')^m + k_2}\mathrm{e}^{-\zeta} \tag{37}$$

with linear operators $\mathcal{L}_1$, $\mathcal{L}_2$, $\mathcal{L}_3$, $\mathcal{L}_4$ and $\mathcal{L}_5$ as

$$\mathcal{L}_1 = h', \quad \mathcal{L}_2 = f'' - f, \quad \mathcal{L}_3 = g'' - g,$$
$$\mathcal{L}_4 = \theta'' - \theta, \quad \mathcal{L}_5 = \phi'' - \phi. \tag{38}$$

The linear operators have the properties

$$\mathcal{L}_1[c_1] = 0,$$
$$\mathcal{L}_2[c_2\mathrm{e}^{\zeta} + c_3\mathrm{e}^{-\zeta}] = 0,$$
$$\mathcal{L}_3[c_4\mathrm{e}^{\zeta} + c_5\mathrm{e}^{-\zeta}] = 0,$$
$$\mathcal{L}_4[c_6\mathrm{e}^{\zeta} + c_7\mathrm{e}^{-\zeta}] = 0,$$
$$\mathcal{L}_5[c_8\mathrm{e}^{\zeta} + c_9\mathrm{e}^{-\zeta}] = 0, \tag{39}$$

where c_i (i =1–9) are constants.

The zeroth-order deformation problems are presented as follows:

$$
\begin{aligned}
&(1-q)\mathcal{L}_1[\hat{h}(\zeta,q)-h_0(\zeta)]\\
&\quad=q\hbar_h\mathcal{N}_1[\hat{h}(\zeta,q),\,\hat{f}(\zeta,q),\,\hat{g}(\zeta,q)],\\
&(1-q)\mathcal{L}_2[\hat{f}(\zeta,q)-f_0(\zeta)]\\
&\quad=q\hbar_f\mathcal{N}_2[\hat{h}(\zeta,q),\,\hat{f}(\zeta,q),\,\hat{g}(\zeta,q)],\\
&(1-q)\mathcal{L}_3[\hat{g}(\zeta,q)-g_0(\zeta)]\\
&\quad=q\hbar_g\mathcal{N}_3[\hat{g}(\zeta,q),\hat{h}(\zeta,q),\,\hat{f}(\zeta,q)],\\
&(1-q)\mathcal{L}_4[\hat{\theta}(\zeta,q)-\theta_0(\zeta)]\\
&\quad=q\hbar_\theta\mathcal{N}_4[\hat{f}(\zeta,q),\hat{g}(\zeta,q),\hat{\theta}(\zeta,q),\hat{h}(\zeta,q),],\\
&(1-q)\mathcal{L}_5[\hat{\phi}(\zeta,q)-\phi_0(\zeta)]\\
&\quad=q\hbar_\Phi\mathcal{N}_5[\hat{f}(\zeta,q),\hat{h}(\zeta,q),\;\hat{g}(\zeta,q),\;\hat{\phi}(\zeta,q)],
\end{aligned}
\tag{40}
$$

$$
\begin{aligned}
&\hat{h}(0,q)=0,\;\hat{f}(0,q)=0,\;\hat{g}(0,q)=1,\;\hat{\theta}(0,q)=1,\\
&\mathrm{Re}^{(1-n)/2(1+n)}(1+r')^m\hat{\phi}'(0,q)=k_2\hat{\phi}(0,q),\\
&\hat{f}(\infty,q)=0,\;\hat{g}(\infty,q)=0,\\
&\hat{\theta}(\infty,q)=0,\;\hat{\phi}(\infty,q)=1,
\end{aligned}
\tag{41}
$$

in which $\hbar_h, \hbar_f, \hbar_g, \hbar_\theta$ and $\hbar_\Phi$ are non-zero auxiliary parameters while the nonlinear operators $\mathcal{N}_1, \mathcal{N}_2, \mathcal{N}_3, \mathcal{N}_4$ and $\mathcal{N}_5$ are given by

$$
\mathcal{N}_1=\frac{\partial\hat{h}(\zeta,q)}{\partial\zeta}+2\hat{f}(\zeta,q)+(\zeta+\alpha)m\epsilon\frac{\partial\hat{f}(\zeta,q)}{\partial\zeta},
\tag{42}
$$

$$
\begin{aligned}
\mathcal{N}_2=&\,\mathrm{Re}^{(1+n)/(1-n)}(1+r')^{2m}\frac{\partial^2\hat{f}(\zeta,q)}{\partial^2\zeta}\\
&-(\zeta+\alpha)m\epsilon\hat{f}(\zeta,q)\frac{\partial\hat{f}(\zeta,q)}{\partial\zeta}\\
&-h\frac{\partial\hat{f}(\zeta,q)}{\partial\zeta}-(\hat{f}(\zeta,q))^2+(\hat{g}(\zeta,q))^2,
\end{aligned}
\tag{43}
$$

$$
\begin{aligned}
\mathcal{N}_3=&\,\mathrm{Re}^{(1+n)/(1-n)}(1+r')^{2m}\frac{\partial^2\hat{g}(\zeta,q)}{\partial^2\zeta}\\
&-(\zeta+\alpha)m\epsilon\hat{f}(\zeta,q)\frac{\partial\hat{g}(\zeta,q)}{\partial\zeta}\\
&-2\hat{f}(\zeta,q)\hat{g}(\zeta,q)-h\frac{\partial\hat{g}(\zeta,q)}{\partial\zeta},
\end{aligned}
\tag{44}
$$

$$
\begin{aligned}
\mathcal{N}_4=&\frac{\gamma}{\mathrm{Pr}}\mathrm{Re}^{(1+n)/(1-n)}(1+r')^{2m}\\
&\times\left(\left(\hat{\theta}(\zeta,q)\frac{\partial^2\hat{\theta}(\zeta,q)}{\partial\zeta^2}+\frac{\partial\hat{\theta}(\zeta,q)}{\partial\zeta}\right)^2\right.\\
&\left.+\frac{1}{\gamma}\frac{\partial^2\hat{\theta}(\zeta,q)}{\partial\zeta^2}\right)-(\zeta+\alpha)m\epsilon\hat{f}(\zeta,q)\\
&\times\frac{\partial\hat{\theta}(\zeta,q)}{\partial\zeta}-\hat{h}(\zeta,q)\frac{\partial\hat{\theta}(\zeta,q)}{\partial\zeta},
\end{aligned}
\tag{45}
$$

$$
\begin{aligned}
\mathcal{N}_5=&\frac{1}{\mathrm{Sc}}\mathrm{Re}^{(1+n)/(1-n)}(1+r')^{2m}\frac{\partial^2\hat{\phi}(\zeta,q)}{\partial\zeta^2}\\
&-(\zeta+\alpha)m\epsilon\frac{\partial\hat{\phi}(\zeta,q)}{\partial\zeta}\\
&-k_1\hat{\phi}(\zeta,q)(1-\hat{\phi}(\zeta,q))^2-h\frac{\partial\hat{\phi}(\zeta,q)}{\partial\zeta},
\end{aligned}
\tag{46}
$$

where $q\in[0,1]$ is the embedding parameter.

3.2 *mth-order deformation problems*

The problems at *m*th-order are expressed as follows:

$$
\begin{aligned}
&\mathcal{L}_1[h_m(\zeta,q)-\chi_m h_{m-1}(\zeta)]=\hbar_h\mathcal{R}_{h,m}(\zeta),\\
&\mathcal{L}_2[f_m(\zeta,q)-\chi_m f_{m-1}(\zeta)]=\hbar_f\mathcal{R}_{f,m}(\zeta),\\
&\mathcal{L}_3[g_m(\zeta,q)-\chi_m g_{m-1}(\zeta)]=\hbar_g\mathcal{R}_{g,m}(\zeta),\\
&\mathcal{L}_4[\theta_m(\zeta,q)-\chi_m\theta_{m-1}(\zeta)]=\hbar_\theta\mathcal{R}_{\theta,m}(\zeta),\\
&\mathcal{L}_5[\phi_m(\zeta,q)-\chi_m\phi_{m-1}(\zeta)]=\hbar_\phi\mathcal{R}_{\phi,m}(\zeta),
\end{aligned}
\tag{47}
$$

$$
\begin{aligned}
&h_m(0)=f_m(0)=g_m(0)=\theta_m(0)=0,\\
&\mathrm{Re}^{(1-n)/2(1+n)}(1+r')^m\phi'_m(0)-k_2\phi_m(0)=0,\\
&f_m(\infty)=g_m(\infty)=\theta_m(\infty)=\phi_m(\infty)=0,
\end{aligned}
\tag{48}
$$

$$
\mathcal{R}_{h,m}(\zeta)=h'_{m-1}+2f_{m-1}+(\zeta+\alpha)m\epsilon f'_{m-1}=0,
\tag{49}
$$

$$
\begin{aligned}
\mathcal{R}_{f,m}(\zeta)=&\,\mathrm{Re}^{(1+n)/(1-n)}(1+r')^{2m}f''_{m-1}\\
&-\sum_{k=0}^{m-1}h_k f'_{m-1-k}+\sum_{k=0}^{m-1}g_m g_{m-1-k}\\
&-(\zeta+\alpha)m\epsilon\sum_{k=0}^{m-1}f_k f'_{m-1-k}\\
&-\sum_{k=0}^{m-1}f_k f_{m-1-k},
\end{aligned}
\tag{50}
$$

$$
\mathcal{R}_{g,m}(\zeta)=\mathrm{Re}^{(1+n)/(1-n)}(1+r')^{2m}g''_{m-1}
$$

$$- (\zeta + \alpha) m\epsilon \sum_{k=0}^{m-1} f_k g'_{m-1-k} - 2 \sum_{k=0}^{m-1} f_m g_{m-1-k} - \sum_{k=0}^{m-1} h_k g'_{m-1-k}, \quad (51)$$

$$\mathcal{R}_{\theta,m}(\zeta) = \frac{\gamma}{\mathrm{Pr}} \mathrm{Re}^{(1+n)/(1-n)} (1+r')^{2m} \times \left(\sum_{k=0}^{m-1} \theta'_k \theta'_{m-1-k} + \frac{\theta''_{m-1}}{\gamma} + \sum_{k=0}^{m-1} \theta_k \theta''_{m-1-k} \right) - \sum_{k=0}^{m-1} h_k \theta'_{m-1-k} - (\zeta + \alpha) \times m\epsilon \sum_{k=0}^{m-1} f_k \theta'_{m-1-k}, \quad (52)$$

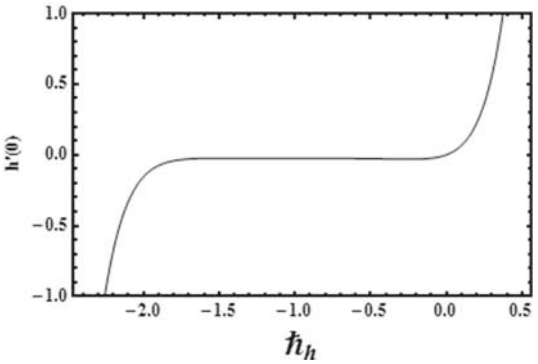

Figure 2. $\hbar$-curve for $h'(0)$.

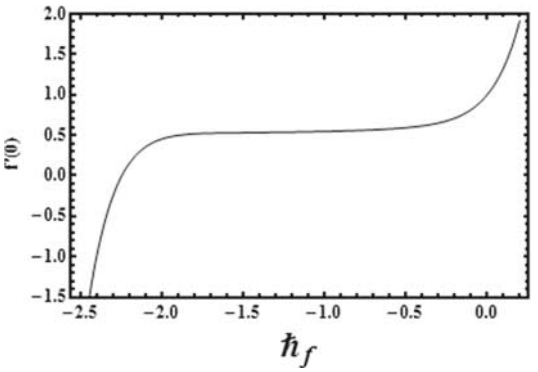

Figure 3. $\hbar$-curve for $f'(0)$.

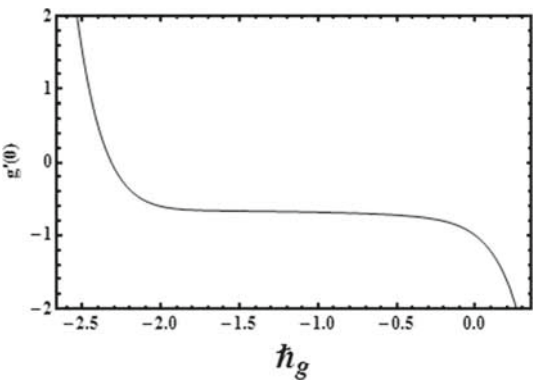

Figure 4. $\hbar$-curve for $g'(0)$.

$$\mathcal{R}_{\phi,m}(\zeta) = \frac{1}{\mathrm{Sc}} \mathrm{Re}^{(1+n)/(1-n)} (1+r')^{2m} \phi''_{m-1} - \sum_{k=0}^{m-1} h_k \phi'_{m-1-k} - (\zeta + \alpha) m\epsilon \phi'_{m-1} + k_1 \sum_{j=0}^{l} \phi_{l-j} \sum_{k=0}^{m-1} \phi_{m-1-k} \phi_k - 2k_1 \sum_{k=0}^{m-1} \phi_k \phi_{m-1-k} - k_1 \phi_{m-1} \quad (53)$$

with

$$\chi_m = \begin{cases} 0, & m \leq 1, \\ 1, & m > 1. \end{cases} \quad (54)$$

The general solutions $(h_m, f_m, g_m, \theta_m, \phi_m)$ are

$$h_m(\zeta) = h^*_m(\zeta) + c_1,$$

$$f_m(\zeta) = f^*_m(\zeta) + c_2 \mathrm{e}^{\zeta} + c_3 \mathrm{e}^{-\zeta},$$

$$g_m(\zeta) = g^*_m(\zeta) + c_4 \mathrm{e}^{\zeta} + c_5 \mathrm{e}^{-\zeta},$$

$$\theta_m(\zeta) = \theta^*_m(\zeta) + c_6 \mathrm{e}^{\zeta} + c_7 \mathrm{e}^{-\zeta},$$

$$\Phi_m(\zeta) = \phi^*_m(\zeta) + c_8 \mathrm{e}^{\zeta} + c_9 \mathrm{e}^{-\zeta}, \quad (55)$$

where $(h^*_m, f^*_m, g^*_m, \theta^*_m, \phi^*_m)$ are particular solutions and the values of constants are

$$c_1 = h^*_m(0), \quad c_3 = -f^*_m(0),$$

$$c_5 = -g^*_m(0), \quad c_7 = -\theta^*_m(0),$$

$$c_9 = \frac{1}{\mathrm{Re}^{(1-n)/2(1+n)} (1+r')^m + k_2} \times \left(\mathrm{Re}^{(1-n)/2(1+n)} (1+r')^m \left. \frac{\partial \phi^*_m(\zeta)}{\partial \zeta} \right|_{\zeta=0} - k_2 \phi^*_m(0) \right),$$

$$c_2 = c_4 = c_6 = c_8 = 0. \quad (56)$$

4. Analysis of the results

4.1 *Convergence of the derived series solutions*

The homotopy analysis method consists of some auxiliary parameters. By assigning appropriate values to these parameters, the convergence region is adjusted. Thus, $\hbar$-curves are plotted to get appropriate ranges of these parameters (see figures 2–6). Valid ranges for $\hbar_h$, $\hbar_f, \hbar_g, \hbar_\theta$ and $\hbar_\phi$ are $-1.7 \leq \hbar_h \leq -0.3, -1.7 \leq \hbar_f \leq -0.9$, $-1.7 \leq \hbar_g \leq -0.7$, $-1.3 \leq \hbar_\theta \leq -0.6$ and $-2.5 \leq \hbar_\phi \leq -0.1$. Also, the series solutions converge when $\hbar_h = -1.1, \hbar_f = -1.4, \hbar_g = -1.3, \hbar_\theta = -1.4$ and $\hbar_\phi = -1$ (see table 1). The values of shear stress at the surface are compared with the previously published results in table 2. Here it is seen that the obtained solutions agree well with the results of Ming *et al* [4] and Xun *et al* [7].

Table 2. Comparison of the present result with Ming *et al* [4] and Xun *et al* [7] when $n = 1$ and $m = 0$.

Order of approximations	$-f'(0)$	$-g'(0)$
Present	0.51093	0.61599
Ming *et al* [4]	0.51021	0.61591
Xun *et al* [7]	0.510231	0.615921

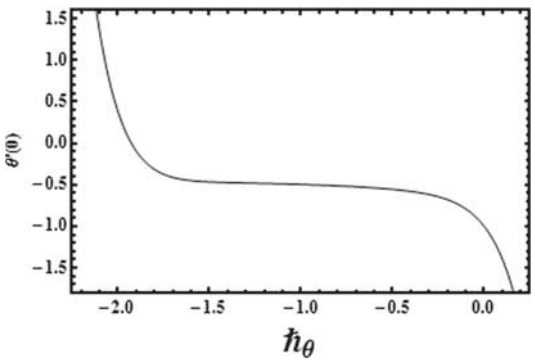

Figure 5. $\hbar$-curve for $\theta'(0)$.

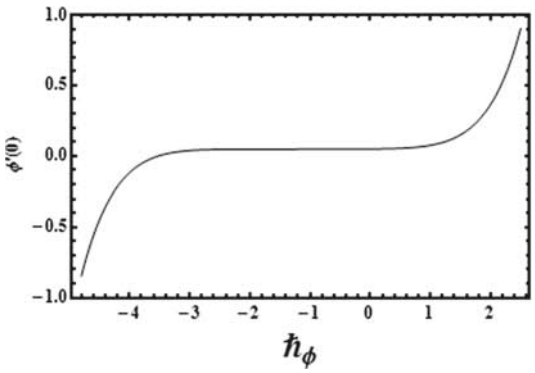

Figure 6. $\hbar$-curve for $\phi'(0)$.

4.2 *Results and discussion*

This section comprises graphical results of the influences of different variables on velocity, temperature and concentration distributions. The influence of variable thickness parameter (n) on axial velocity ($h(\zeta)$) and radial velocity ($f'(\zeta)$) components are shown in figures 7 and 8. A larger value of n causes decrease in radius R_0. This results in less resistance and hence velocity is enhanced. Also, a negative value of $h(\zeta)$ implies that the fluid is moving in a vertically downward direction. Radial velocity ($f'(\zeta)$) is an increasing function of dimensionless parameter ϵ, as shown in figure 9. When the value of ϵ is increased then the feature radius R_0 reduces and less fluid particles are left in contact

Table 1. Various order of approximations for converging solutions when $\alpha = 1.5, n = m = 1, \epsilon = 0.03$, Re=0.2, $r' = 0.02$, $\gamma = 0.05$, Pr $= 0.9$, $k_1 = k_2 = 0.1$ and Sc $= 0.9$.

Order of approximations	$-h'(0)$	$f'(0)$	$-g'(0)$	$-\theta'(0)$	$\phi'(0)$
1	0.0495	0.618	0.762	0.559	0.0474
5	0.0255	0.554	0.691	0.501	0.0472
7	0.0246	0.541	0.677	0.484	0.0470
12	0.0237	0.525	0.658	0.457	0.0468
16	0.0237	0.520	0.650	0.444	0.0467
21	0.0237	0.515	0.643	0.433	0.0466
25	0.0237	0.515	0.639	0.427	0.0466
30	0.0237	0.515	0.639	0.421	0.0466
35	0.0237	0.515	0.639	0.416	0.0466
38	0.0237	0.515	0.639	0.415	0.0466
40	0.0237	0.515	0.639	0.415	0.0466
45	0.0237	0.515	0.639	0.415	0.0466
50	0.0237	0.515	0.639	0.415	0.0466

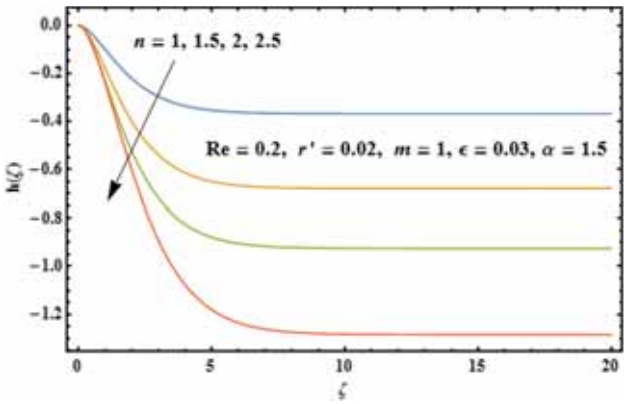

Figure 7. Variation in $h(\zeta)$ by changing n.

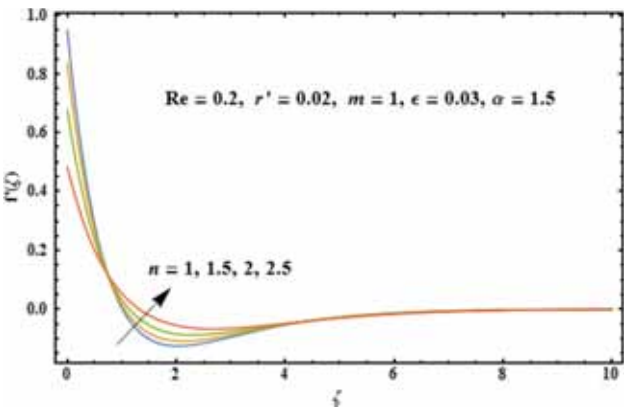

Figure 8. Variation in $f'(\zeta)$ by changing n.

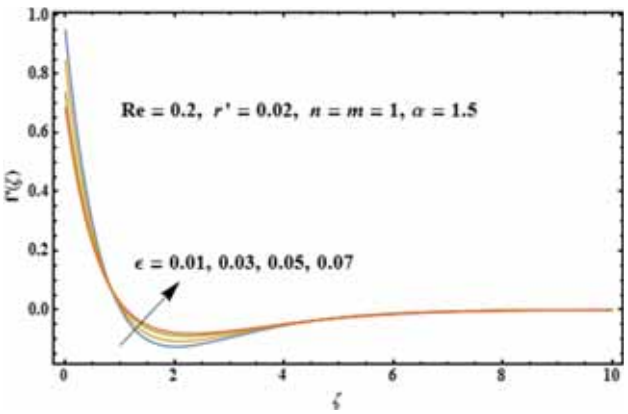

Figure 9. Variation in $f'(\zeta)$ by changing ϵ.

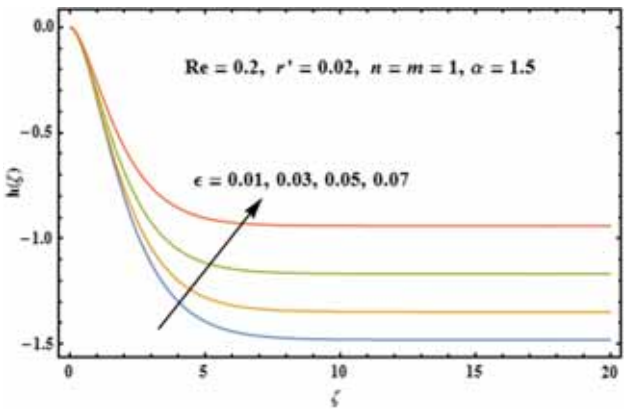

Figure 10. Variation in $h(\zeta)$ by changing ϵ.

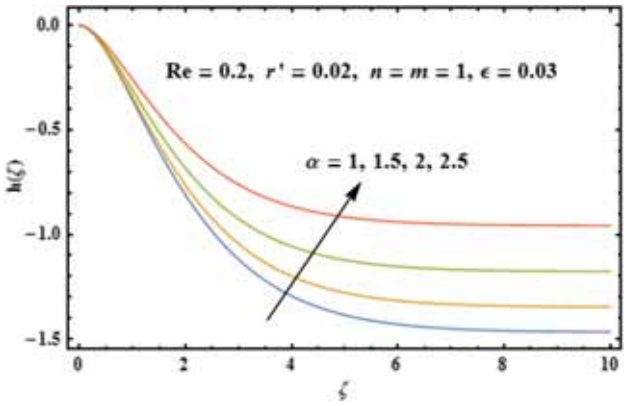

Figure 11. Variation in $h(\zeta)$ by changing α.

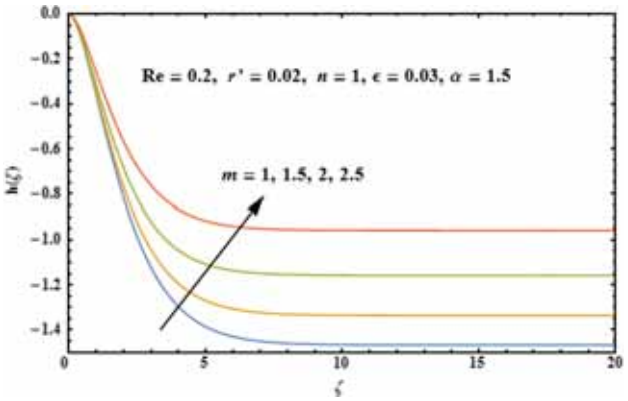

Figure 12. Variation in $h(\zeta)$ by changing m.

with disk. But the opposite behaviour of ϵ is observed on the axial velocity ($h(\zeta)$) profile (see figure 10). An increment in disk thickness coefficient (α) results in a decrease of $h(\zeta)$ (see figure 11). Figures 12 and 13 show that the disk thickness index (m) has opposite impact on axial and radial velocity components. An increase in m causes an increase in radial velocity while the axial velocity decays. The influence of Reynolds number (Re) on $f'(\zeta)$ is depicted in figure 14. Clearly, the radial velocity enhances for increasing Re.

Figures 15–18 depict the influence of variable thickness parameters (n), constant number (ϵ), disk thickness index (m) and Re on tangential velocity ($g(\zeta)$). Figures 15 and 16 show that tangential velocity increases when both m and ϵ are enhanced. Also, the tangential velocity enhances by increasing n (see figure 17). It is

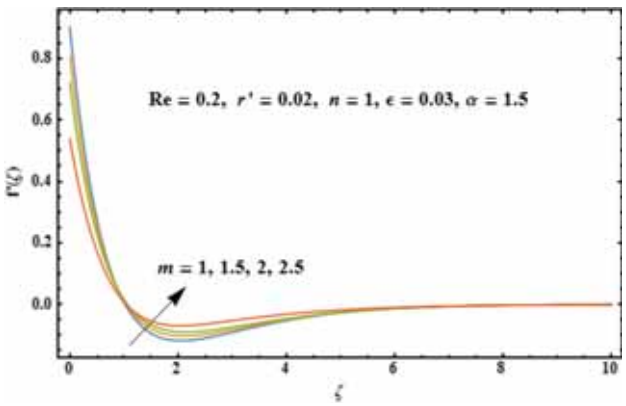

Figure 13. Variation in $f'(\zeta)$ by changing m.

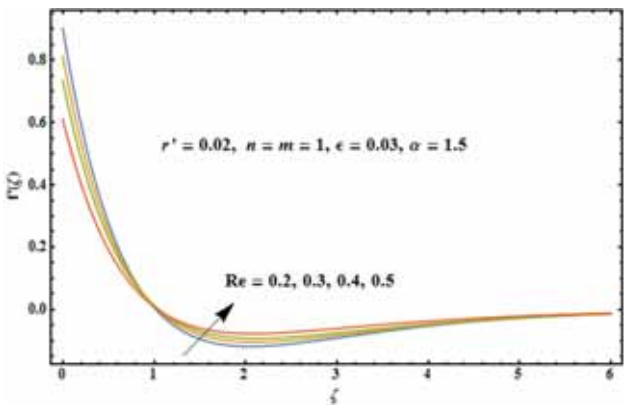

Figure 14. Variation in $f'(\zeta)$ by changing Re.

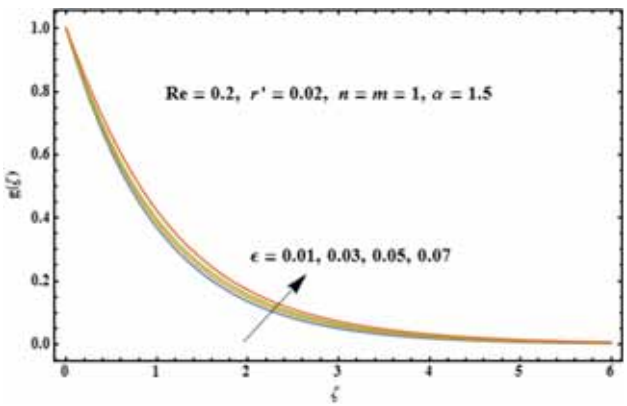

Figure 15. Variation in $g(\zeta)$ by changing ϵ.

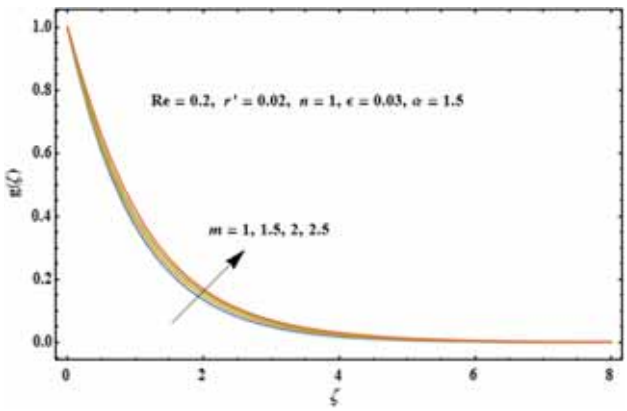

Figure 16. Variation in $g(\zeta)$ by changing m.

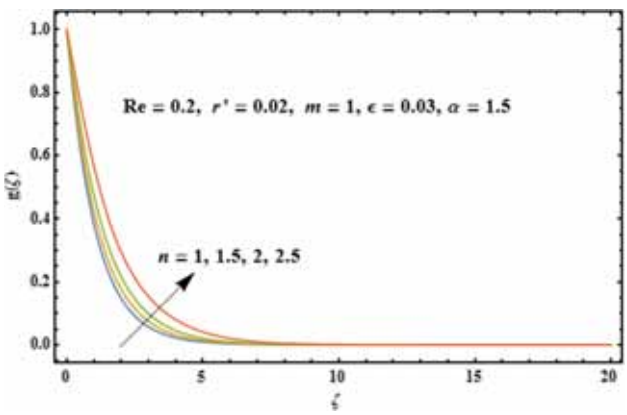

Figure 17. Variation in $g(\zeta)$ by changing n.

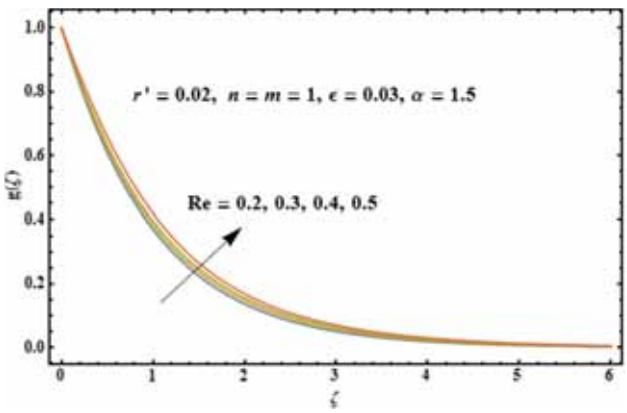

Figure 18. Variation in $g(\zeta)$ by changing Re.

due to the reason that the feature radius (R_0) decreases for larger n and hence resistance enhances. Re is directly related to $g(\zeta)$ (see figure 18).

The influence of Prandtl number (Pr) on temperature distribution ($\theta(\zeta)$) is shown in figure 19. Physically, thermal diffusivity is inversely related to Pr. Hence, the fluid with large Pr diffuses slowly compared to the fluid with lower Pr. Such difference consequently results in reduced temperature and thermal boundary layer thickness. Figure 20 analyses the impact of variable thickness parameter (n) against $\theta(\zeta)$. Graphical result shows that the thickness of a disk decreases for large values of n and thus temperature decreases. The impact of disk thickness index (m) on temperature distribution is observed in figure 21. Clearly, the temperature profile enhances for increasing m. Also for large values of constant ϵ,

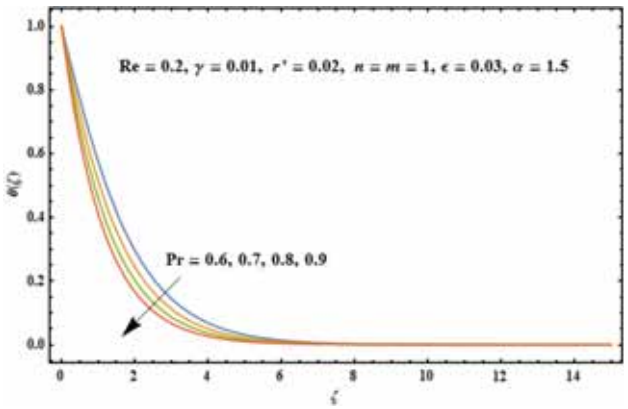

Figure 19. Variation in $\theta(\zeta)$ by changing Pr.

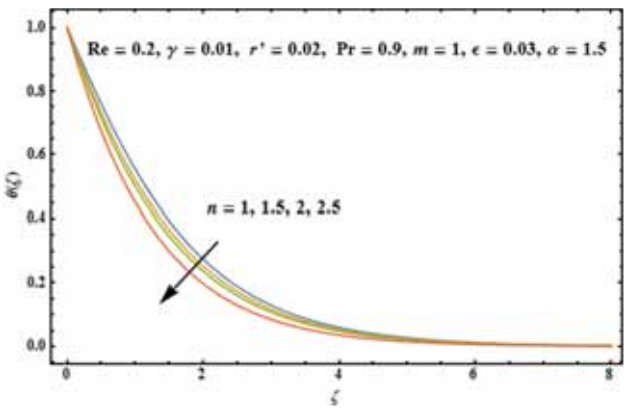

Figure 20. Variation in $\theta(\zeta)$ by changing n.

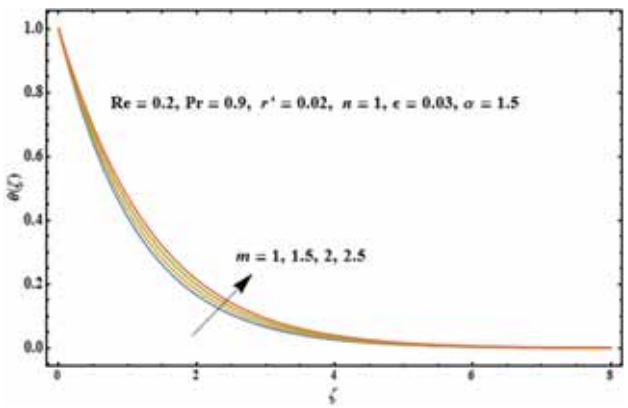

Figure 21. Variation in $\theta(\zeta)$ by changing m.

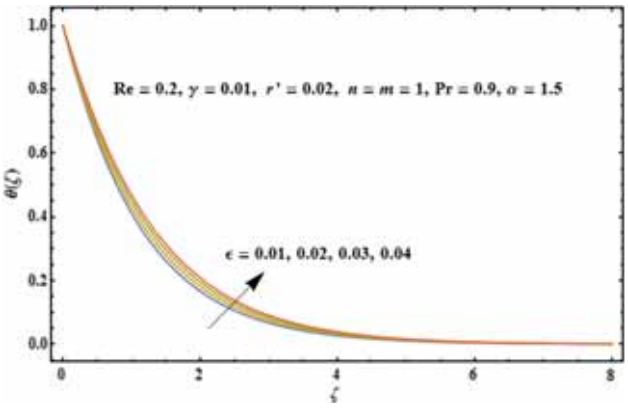

Figure 22. Variation in $\theta(\zeta)$ by changing ϵ.

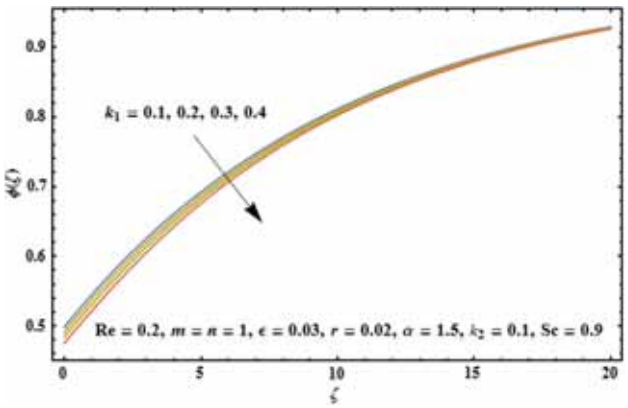

Figure 23. Variation in $\phi(\zeta)$ by changing k_1.

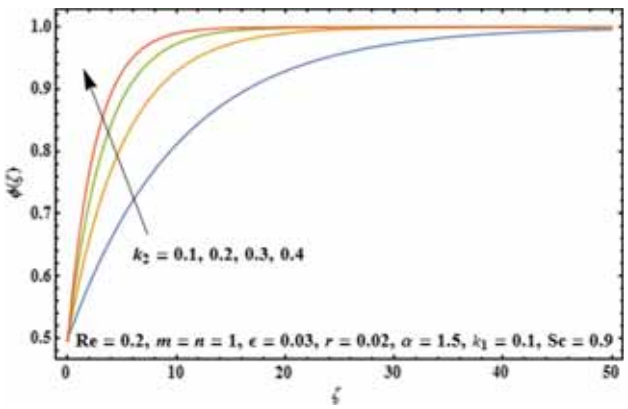

Figure 24. Variation in $\phi(\zeta)$ by changing k_2.

$\theta(\zeta)$ enhances (figure 22). It is due to the fact that feature radius (R_0) is dependent on ϵ. Clearly, there is a reduction in R_0 when ϵ increases. This results in less area of contact of fluid particles and the disk. Hence, both heat transfer and temperature are enhanced.

The behaviour of Schmidt number (Sc), homogeneous reaction parameter (k_1) and heterogeneous reaction parameter (k_2) on concentration distribution ($\phi(\zeta)$) is depicted in figures 23–25. For enhancing the value of k_1, there occurs a fast consumption of reactants which consequently decreases the concentration. The opposite behaviour of k_2 on $\phi(\zeta)$ is analysed in figure 24. It is due to the fact that mass diffusivity is inversely related to k_2 and thus a larger value of k_2 consequently increases the concentration. Figure 25 illustrates the impact of Sc on concentration field. The increment in

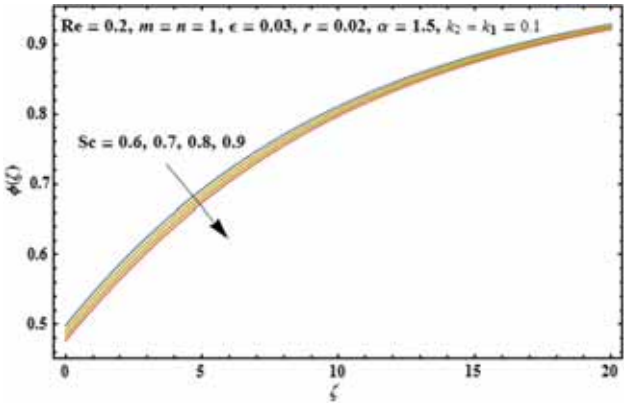

Figure 25. Variation in $\phi(\zeta)$ by changing Sc.

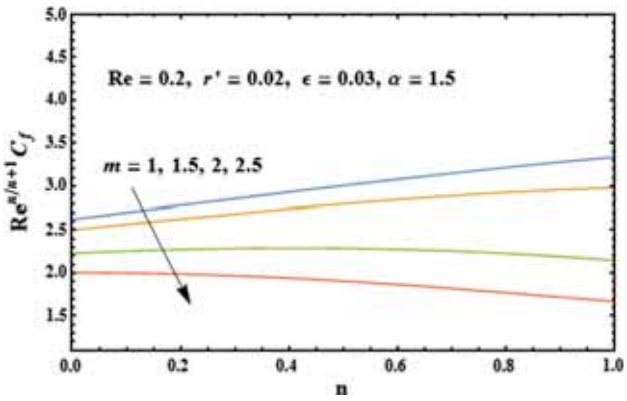

Figure 26. Variation in $C_f \mathrm{Re}^{n/(n+1)}$ by changing m.

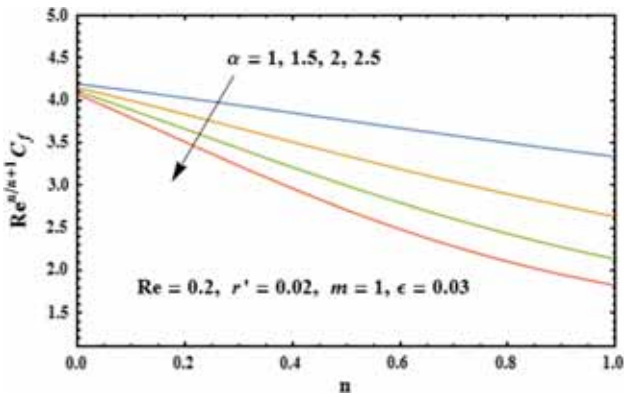

Figure 27. Variation in $C_f \mathrm{Re}^{n/(n+1)}$ by changing α.

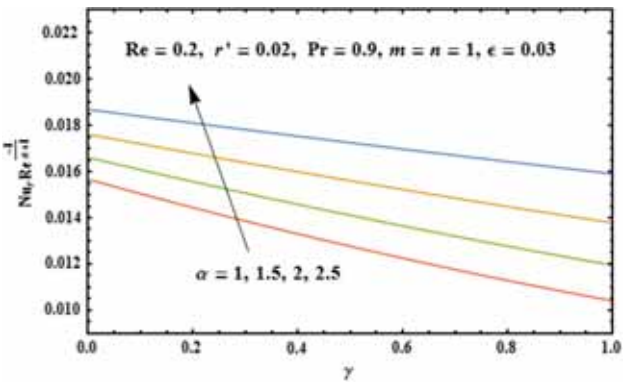

Figure 28. Plots of α against $\mathrm{Nu}_r \mathrm{Re}^{-1/(n+1)}$.

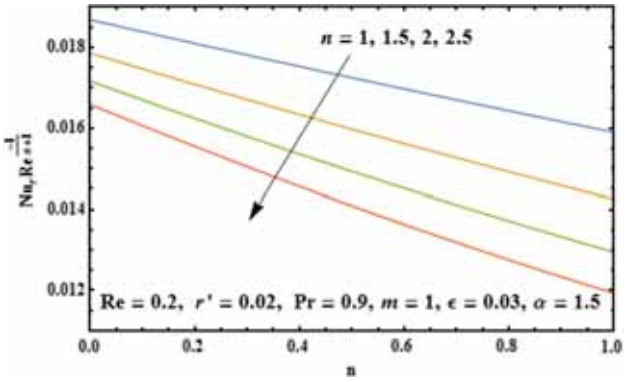

Figure 29. Plots of n against $\mathrm{Nu}_r \mathrm{Re}^{-1/(n+1)}$.

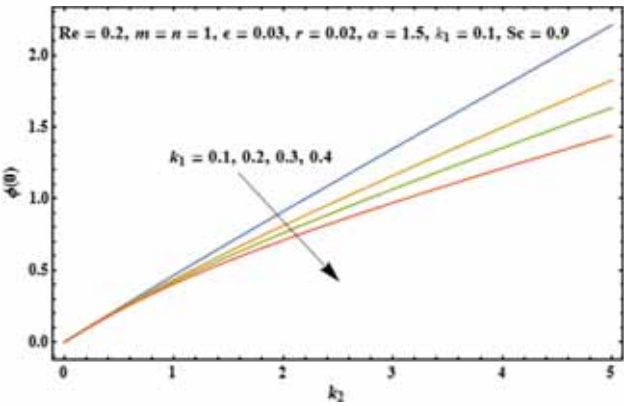

Figure 30. Plots of k_2 against $\phi(0)$.

Sc reduces the molecular diffusivity and hence concentration decreases.

Figures 26 and 27 are plotted to show the impact of thickness coefficient of the disk (α) and disk thickness index (m) on the skin friction coefficient ($C_f \mathrm{Re}^{n/(n+1)}$). It is observed that the surface drag force decays with an increase in m and α while this behaviour is noted for increasing values of n. Also, figures 28 and 29 present the Nusselt number ($\mathrm{Nu}_r \mathrm{Re}^{-1/(n+1)}$) for larger γ. Clearly, the Nusselt number enhances when α increases and it decreases with decrease in n. For larger values of k_1, more reactants are consumed and hence the surface concentration decreases (see figure 30).

5. Concluding remarks

The effect of homogeneous and heterogeneous reactions in fluid flow by a rotating disk with variable thickness is discussed here. The main points are highlighted here:

- Both axial and radial velocities are enhanced when the variable thickness parameter increases.
- Temperature distribution is an increasing function of the disk thickness index.
- With an increase in homogeneous reaction parameter the concentration decreases, while it increases with larger heterogeneous reaction parameter.
- Higher values of disk thickness index and thickness coefficient of the disk correspond to a decrease in the surface drag force.
- Larger values of disk thickness coefficient enhance the heat transfer rate.

References

[1] T V Karman, *Z. Angew. Math. Mech.* **1**, 233 (1921)
[2] K Stewartson, *Proc. Camb. Phil. Soc.* **49**, 333 (1953)
[3] S K Kumar, W I Tacher and L T Watson, *Appl. Math. Model.* **13**, 494 (1989)
[4] C Y Ming, L C Zheng and X X Zhang, *Int. Commun. Heat Mass* **38**, 280 (2011)
[5] M Turkyilmazoglu, *Comput. Fluid* **90**, 51 (2014)
[6] P V S Narayana, B Venkateswarlu and S Venkataramana, *Heat Transf. Asian Res.* **44**, 21101 (2015)
[7] S Xun, J Zhao, L Zheng, X Chen and X Zhang, *Int. J. Heat Mass Transf.* **103**, 1214 (2016)
[8] D Pal and S Chatterjee, *Appl. Math. Comput.* **219**, 7556 (2013)
[9] K Vajravelu, K V Prasad and C Ng, *Nonlinear Anal. Real World Appl.* **14**, 455 (2013)
[10] S A Shehzad, A Alsaedi, T Hayat and M S Alhuthali, *PLoS One* **8**, e78240 (2013)
[11] T Hayat, S A Shehzad and A Alsaedi, *Appl. Math. Mech.* **34**, 823 (2013)
[12] T Hayat, A Shafiq, A Alsaedi and S Asghar, *AIP Adv.* **5**, 087108 (2015)
[13] B Venkateswarlu and P V S Narayana, *Front. Heat Mass Transf.* **7**, 16 (2016)
[14] T Hayat, M I Khan, M Farooq, A Alsaedi, M Waqas and T Yasmeen, *Int. J. Heat Mass Transf.* **99**, 702 (2016)
[15] G Sarojamma, R V Lakshmi, P V S Narayana and K Vajravelu, *J. Appl. Comput. Mech.* **5**, 441 (2019)
[16] I Shufrin and M Eisenberger, *Int. J. Solids Struct.* **42**, 1225 (2005)
[17] T G Fang, J Zhang and Y F Zhong, *Appl. Math. Comput.* **218**, 7241 (2012)
[18] S V Subhashini, R Sumathi and I Pop, *Int. Commun. Heat Mass* **48**, 61 (2013)
[19] T Hayat, M Farooq, A Alsaedi and F AlSolamy, *AIP Adv.* **5**, 087159 (2015)
[20] T Hayat, G Bashir, M Waqas and A Alsaedi, *J. Mol. Liq.* **44**, 844 (2016)
[21] J H Merkin, *Math. Comput. Model.* **24**, 125 (1996)
[22] M A Chaudhary and J H Merkin, *Fluid Dyn. Res.* **16**, 311 (1995)
[23] W A Khan and I Pop, *Commun. Nonlinear Sci. Numer. Simul.* **15**, 3435 (2010)
[24] T Hayat, M Awais, S Ambreen and A A Hendi, *Nonlinear Anal. Modell. Control* **17**, 47 (2012)
[25] W A Khan and I Pop, *ASME J. Heat Transf.* **134**, 1 (2012)
[26] T Hayat, A Tanveer, F Alsaadi and N D Alotaibi, *AIP Adv.* **5**, 067172 (2015)
[27] T Hayat, M Imtiaz, A Alsaedi and S Almezal, *J. Magn. Magn. Mater.* **401**, 296 (2016)
[28] T Hayat, S Qayyum, M Imtiaz and A Alsaedi, *PLoS One* **11**, e0148662 (2016)
[29] T Hayat, K Muhammad, M I Khan and A Alsaedi, *Pramana – J. Phys.* **92**: 57 (2019)
[30] S J Liao, *Beyond perturbation* (Springer and Higher Education Press, Heidelberg, 2012)
[31] S Abbasbandy, M Yurusoy and H Gulluce, *Math. Comput. Appl.* **19**, 124 (2014)
[32] M Turkyilmazoglu, *Filomat* **30**, 1633 (2016)
[33] Y Lin, L Zheng and G Chen, *Powder Technol.* **274**, 332 (2016)
[34] S Qayyum, M Imtiaz, A Alsaedi and T Hayat, *Chin. J. Phys.* **56**, 2404 (2018)
[35] M Imtiaz, A Kiran, T Hayat and A Alsaedi, *J. Braz. Soc. Mech. Sci. Eng.* **41**, 149 (2019)